From Condensed Lanthanide Coordination Solids to Microporous Frameworks Having Accessible Metal Sites

Theresa M. Reineke, Mohamed Eddaoudi, Michael Fehr,† Douglas Kelley,† and O. M. Yaghi*

Contribution from the Supramolecular Design and Discovery Group, Department of Chemistry and Biochemistry, Arizona State University, Box 871604, Tempe, Arizona 85287-1604, and Nalco Chemical Company, One Nalco Center, Naperville, Illinois 60563

Received October 12, 1998

Abstract: The combination of terbium nitrate and 1,4-benzenedicarboxylic acid (H_2BDC) in the presence of triethylamine yields the compound $Tb_2(BDC)_3\cdot(H_2O)_4$, which has an extended nonporous structure constructed from copolymerized BDC and Tb(III) units. The multidentate functionality of BDC and the tendency of Tb to have a high coordination number has allowed water to act as a terminal ligand to Tb in the structure. Upon thermally liberating the water ligands, a microporous material, $Tb_2(BDC)_3$, is achieved, which has extended 1-D channels and the same framework structure as that of the as-synthesized solid as evidenced by XRPD. Water sorption isotherm data proves that $Tb_2(BDC)_3$ has permanent microporosity, and points to the presence of accessible metal sites within the pores, which also allows the sorption of ammonia to give $Tb_2(BDC)_3\cdot(NH_3)_4$. Luminescence lifetime measurements confirm that resorbed water and sorbed ammonia are bound to Tb and that they give distinctly different decay constants.

Introduction

The recent exponential growth in the synthesis and characterization of metal−organic open frameworks has provided spectacular examples of how the metal-ion geometry and the organic molecule symmetry can be exploited for designing materials with unusual structures and properties.[1,2] The successful realization of synthetic strategies leading to robust metal−organic open networks coupled with the subsequent study of their gas sorption isotherms,[3] guest inclusion from liquids,[4] and ion-exchange properties[5] have established microporosity in this new class of porous materials. Relevant to this progress are important factors related to the amenability of the building block approach to allowing *molecular structural* and *reactivity* properties to be translated into the assembled solid. Illustrative examples extracted from Zn(II) coordination chemistry are schematically shown in Figure 1a−d. Discrete dinuclear and trinuclear metal−organic cluster aggregates **a** and **b** are produced when *mono*-carboxylate ligands such as acetate[6] and crotonate[7] are employed, respectively. Using multidentate carboxylates, such as the trifunctional 1,3,5-benzenetricarboxylate (BTC) and the bifunctional 1,4-benzenedicarboxylate (BDC), polymerizes these aggregates into extended open frameworks, $Zn_2(BTC)(NO_3)\cdot(H_2O)(C_2H_5OH)_5$ and $Zn_2(BDC)_3\cdot 6CH_3OH$, having pores of 14 and 7 Å in diameter, respectively.[4a,8] These frameworks contain the $M_2O_6C_2$ and $M_3O_{10}C_4$ core motifs, which are strikingly similar to those observed in the discrete molecular complexes (compare **a** and **c** for the Zn−BTC and **b** and **d** for Zn−BDC frameworks). Translating the structural attributes of such molecular metal−carboxylate clusters into extended metal−organic open frameworks has been a key to imparting stability and rigidity onto the resulting

† Nalco Chemical Company.

(1) (a) Batten, S. R.; Robson, R. *Angew. Chem., Int. Ed.* **1998**, *37*, 1460−1494. (b) Yaghi, O. M.; Li, H.; Davis, C.; Richardson, D.; Groy, T. L. *Acc. Chem. Res.* **1998**, *31*, 474−484. (c) Venkataraman, D.; Lee, S.; Moore, J. S.; Zhang, P.; Hirsch, K. A.; Gardner, G. B.; Covey, A. C.; Prentice, C. L. *Chem. Mater.* **1996**, *8*, 2030−2040. (d) MacGillivray, L. R.; Groeneman, R. H.; Atwood, J. L. *J. Am. Chem. Soc.* **1998**, *120*, 2676−2677. (e) Kepert, C. J.; Rosseinsky, M. J. *J. Am. Chem. Soc., Chem. Commun.* **1998**, 31−32. (f) Leu, F.; Tilley, T. D. *J. Am. Chem. Soc., Chem. Commun.* **1998**, 103−104. (g) Vaid, T. P.; Lobkovsky, E. B.; Wolczanski, P. T. *J. Am. Chem. Soc.* **1997**, *119*, 8742−8743. (h) Zaworotko, M. J. *Nature* **1997**, *386*, 220. (i) Mallouk, T. E. *Nature* **1997**, *387*, 350. (j) Kondo, M.; Yoshitomi, T.; Seki, K.; Matsuzaka, H.; Kitagawa, S. *Angew. Chem., Int. Ed. Engl.* **1997**, *36*, 1725−1727. (k) Brunet, P.; Simard, M.; Wuest, J. D. *J. Am. Chem. Soc.* **1997**, *119*, 2737−2738. (l) Lu, J.; Paliwala, T.; Lim, S. C.; Yu, C.; Niu, T.; Jacobson, A. J. *Inorg. Chem.* **1997**, *36*, 923−929. (m) Whang, D.; Kim, K. *J. Am. Chem. Soc.* **1997**, *119*, 451−452. (n) Keller, S. W. *Angew. Chem., Int. Ed. Engl.* **1997**, *36*, 247−248. (o) Carlucci, L.; Ciani, G.; Gudenberg, D. W. V.; Proserpio, D. M.; Sironi, A. *J. Am. Chem. Soc., Chem. Commun.* **1997**, 631−632.

(2) (a) Brousseau, L. C., III; Aurentz, D. J.; Benesi, A. J.; Mallouk, T. E. *Anal. Chem.* **1997**, *69*, 688−694. (b) Reis, K. P.; Joshi, V. K.; Thompson, M. E. *J. Catal.* **161**, 62−67 1996. (c) Ramprasad, D.; Pez, G. P.; Toby, B. H.; Markley, T. J.; Pearlstein, R. M. *J. Am. Chem. Soc.* **1995**, *117*, 10694−10701. (d) Yaghi, O. M. U.S. Patent 5,648,508, July 15, 1997. (e) Baron, V.; Gillon, B.; Cousson, A.; Mathonière, C.; Kahn, O.; Grand, A.; Öhrström, L.; Delley, B.; Bonnet, M.; Boucherle, J. *J. Am. Chem. Soc.* **1997**, *119*, 3500−3506. (f) Sato, O.; Iyoda, T.; Fujishima, A.; Hashimoto, K. *Science* **1996**, *271*, 49−51. (g) Aumüller, A.; Erk, P.; Klebe, G.; Hünig, S.; von Schütz, J. U.; Werner, H. *Angew. Chem., Int. Ed. Engl.* **1986**, *25*, 740−741. (h) Munakata, M.; Wu, L. P.; Kuroda-Sowa, T.; Maekawa, M.; Suenaga, Y.; Furuichi, K. *J. Am. Chem. Soc.* **1996**, *118*, 3305−3306. (i) Tamaki, H.; Zhong, Z. J.; Matsumoto, N.; Kida, S.; Koikawa, M.; Achiwa, N.; Hashimoto, Y.; Okawa, H. *J. Am. Chem. Soc.* **1992**, *114*, 6974−6979.

(3) Li, H.; Eddaoudi, M.; Groy, T. L.; Yaghi, O. M. *J. Am. Chem. Soc.* **1998**, *120*, 8571−8572.

(4) (a) Yaghi, O. M.; Davis, C. E.; Li, G.; Li, H. *J. Am. Chem. Soc.* **1997**, *119*, 2861−2868. (b) Yaghi, O. M.; Li, G.; Li, H. *Nature*, **1995**, *378*, 703−706.

(5) Yaghi, O. M.; Li, H. *J. Am. Chem. Soc.* **1996**, *118*, 295−296.

(6) (a) Birnbaum, A.; Cotton, F. A.; Dori, Z.; Kapon, M. *Inorg. Chem.* **1984**, *23*, 1617−1619. (b) Malik, M. A.; Motevalli, M.; O'Brien, P. *Inorg. Chem.* **1995**, *34*, 6223−6225.

(7) (a) Clegg, W.; Little, I. R.; Straughan, B. P. *J. Chem. Soc., Dalton Trans.* **1986**, 1283−1288. (b) Clegg, W.; Little, I. A.; Straughan, B. P. *J. Chem. Soc., Chem. Commun.* **1985**, 73−74.

(8) Li, H.; Davis, C. E.; Groy, T. L.; Kelley, D. G.; Yaghi, O. M. *J. Am. Chem. Soc.* **1998**, *120*, 2186−2187.

10.1021/ja983577d CCC: $18.00
Published on Web 02/04/1999

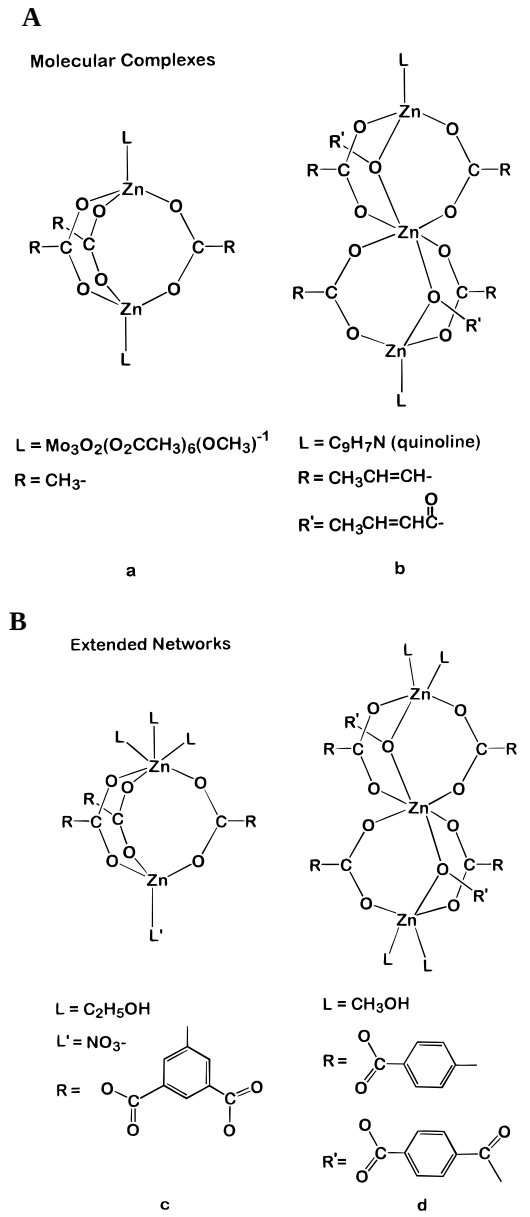

Figure 1. Schematic representations to illustrate the close structural relationships between molecular clusters (A) and extended metal−organic solids (B).

network and to providing means for preventing the formation of interpenetrated nets.[1b]

These multinuclear aggregates also provide an opportunity to translate molecular reactivity into extended frameworks. In that, the geometric constraints placed on the metal center by virtue of extensive multidentate carboxylate bonding that often allows a terminal ligand to occupy non-carboxylate coordinated sites (L and L′) on the metal ion **a**−**d**. In the extended networks **c** and **d**, such ligands ultimately point toward the center of the channels into the void space. Thus, they can be removed with great facility, especially when weakly coordinating, leaving behind Lewis acid sites that are potentially capable of highly selective binding of incoming guest molecules, for the inclusion process is no longer based solely on the shape and size of guests but on their functionality as well.

In this report we demonstrate how the structural and reactivity principles just outlined for the zinc−carboxylate system can be useful in the conversion of condensed lanthanide−organic solids into microporous networks. Although the assembly of transition-metal−organic open frameworks is now well-established, the analogous chemistry of the lanthanide metal ions remains undeveloped.[9] This is attributed to the tendency of these ions for high coordination that favors the formation of condensed structures.[10] We show here that water ligands bonded to lanthanide ions in the condensed nonporous extended 3-D structure of $M_2(BDC)_3 \cdot (H_2O)_4$ (M =Eu and Tb) can be liberated from the solid to yield a *microporous* framework, $M_2(BDC)_3$, which is stable up to 450 °C and has the same framework topology as the original solid. Water sorption isotherm measurements point to the presence of a periodic array of accessible metal centers decorating the channels, which result upon water dissociation. Luminescence lifetime studies performed on the hydrated, dehydrated, and the ammonia-sorbed solids reveal distinctly different decay constants for each material, serving as a first step to developing the use of accessible metal centers in chemical sensing applications.

Experimental Section

Materials and Methods. Terbium(III) nitrate pentahydrate, europium(III) nitrate pentahydrate, and 1,4-benzenedicarboxylic acid (H_2-BDC) were purchased from Aldrich Chemical Co. and used as received, without further purification. Elemental microanalyses of all products were performed on crystalline samples by the School of Chemical Sciences Microanalytical Laboratory at the University of Illinois-Urbana and by the Arizona State University Materials Facility using a Perkin-Elmer 2400 CHNS analyzer. Thermogravimetric (TG) analysis was performed under He at a scan rate of 0.5 °C/min using a Setaram TG92 system.

Fourier transform infrared (FT-IR) spectra were measured from KBr pellets using a Nicolet FT-IR Impact 400 system. Absorptions are described as follows: very strong (vs), strong (s), medium (m), weak (w), shoulder (sh), and broad (br). X-ray powder diffraction (XRPD) data was recorded on a Rigaku D/Max-IIB diffractometer at 50 kV, 30 mA for Cu Kα,(λ = 1.5406 Å) with a scan speed of 2°/min and a step size of 0.02° in 2θ. Calculated XRPD patterns were produced using the SHELXTL-XPOW program and the single-crystal data.

Preparation of Compounds. The synthetic methods used to obtain pure crystalline samples of the compounds, and their initial characterization are described here. Unless otherwise indicated, all reactions and purification steps were performed under aerobic conditions.

$Tb_2(BDC)_3 \cdot (H_2O)_4$. An aqueous mixture (9 mL) containing H_2BDC (0.025 g, 0.15 mmol) and $Tb(NO_3)_3 \cdot 5H_2O$ (0.065 g, 0.15 mmol) was placed in a Parr Teflon-lined stainless steel vessel (23 mL). Triethylamine (0.30 mL, 2.1 mmol) was added to this heterogeneous mixture, and the vessel was sealed and heated to 140 °C for 12 h and then cooled to room temperature at a rate of 0.1 °C/min. Small colorless crystals of the product were collected and washed with 3 × 10 mL of Nanopure water and allowed to dry in air overnight, yielding 0.030 g (68% yield). The product is stable in air and insoluble in water and all common organic solvents such as ethanol, acetonitrile, tetrahydrofuran, 1,2-dichloroethane, acetone, and *N*,*N*′-dimethylformamide. Anal. Calcd For $C_{24}H_{20}O_{16}Tb_2 = Tb_2(BDC)_3 \cdot (H_2O)_4$ C, 32.67; H, 2.28; N, 0.00. Found C, 32.74; H, 2.21; N, 0.09. FT-IR (KBr, 3500−400 cm^{-1}): 3460 (br), 3059 (sh), 1618 (m), 1591 (m), 1552 (vs), 1512 (vs), 1427 (s), 1407 (s), 1315 (sh), 1163 (w), 1131 (w), 1104 (w), 1025 (w), 894 (w), 841 (w), 775 (m), 749 (m), 617, (m), 591 (m), 565 (m), 538 (m), 512 (m), 426 (m). The europium analogue of this compound was also prepared using an identical procedure and found to have the same composition

(9) Kiritsis, V.; Michaelides, A.; Skoulika, S.; Golhen, S.; Ouahab, L. *Inorg. Chem.* **1998**, *37*, 3407−3410.

(10) (a) Wu, L. P.; Munakata, M.; Kuroda-Sowa, T.; Maekawa, M.; Suenaga, Y. *Inorg. Chim. Acta* **1996**, *249*, 183−189. (b) Seddon, J. A.; Jackson, A. R. W.; Kresinski, R. A.; Platt, W. G. *Polyhedron* **1996**, *15*, 1899−1902. (c) Ribeiro, S. J. L.; Gonçalves, R. R.; de Oliveira, L. F. C.; Santos, P. S. *J. Alloys Compd* **1994**, *216*, 61−66. (d) Huskowska, E.; Glowiak, T.; Legendziewicz, J.; Oremek, G. *J. Alloys and Compd* **1992**, *179*, 13−25. (e) Zhibang, D.; Gecheng, W.; Zhongshen, J.; Jiazan, N. *J. Less-Common Met.* **1991**, *171*, L1-L3. (f) Yaghi, O. M.; Li, H.; Groy, T. L. *Z. Kristallogr.* **1997**, *212*, 457−458.

Table 1. XRPD Data for $Tb_2(BDC)_3 \cdot (H_2O)_4$ Starting Material, **1**, and $Eu_2(BDC)_3 \cdot (H_2O)_4$, **2**, Including *hkl*, *d*-Spacing (Å), Intensity (I/I_o), and Full Width at Half-Maximum (fwhm)

	1					**2**		
	calcd		obsd					
hkl	*d*-spacing	I/I_o (%)	*d*-spacing	I/I_o (%)	fwhm	*d*-spacing	I/I_o (%)	fwhm
0$\bar{1}$0	9.624	100	9.668	100	0.174	9.689	100	0.175
0$\bar{1}\bar{1}$	7.795	6	7.824	6	0.379	7.866	7	0.298
$\bar{1}$00	6.006	48	6.046	49	0.192	6.062	51	0.193
$\bar{1}$10	5.652	31	5.683	27	0.196	5.705	28	0.216
002	4.923	19	4.940	21	0.219	4.962	19	0.540
020	4.812	20	4.828	36	0.295	4.834	37	0.334
$\bar{1}$10	4.676	16	4.702	16	0.257	4.706	19	0.218
$\bar{1}$20	4.208	10	4.219	10	0.277	4.231	14	0.199
012	4.037	19	4.048	16	0.235	4.063	22	0.197
0$\bar{2}$2	3.897	15	3.904	15	0.178	3.924	15	0.236
$\bar{1}$02	3.692	7	3.711	16	0.257	3.723	16	0.318
$\bar{1}$12	3.592	20	3.610	21	0.199	3.625	20	0.236
$\bar{1}\bar{2}$2	3.461	7	3.432	6	0.278	3.437	8	0.419
$\bar{1}$22	3.106	8	3.119	18	0.236	3.129	19	0.238
$\bar{2}$00	3.003	5	3.006	13	0.378	3.018	15	0.338
$\bar{1}\bar{1}$3	2.910	18	2.929	18	0.316	2.942	22	0.298
1$\bar{3}$2	2.875	10	2.873	10	0.237	2.886	12	0.217

Table 2. XRPD Data for $Tb_2(BDC)_3$, **3**, Regenerated $Tb_2(BDC)_3 \cdot (H_2O)_4$, **4**, and $Tb_2(BDC)_3 \cdot (NH_3)_4$, **5**, Including, *d*-Spacing, (Å), Intensity (I/I_o), and Full Width at Half-Maximum (fwhm)

3			**4**			**5**		
d-spacing	I/I_o (%)	fwhm	*d*-spacing	I/I_o (%)	fwhm	*d*-spacing	I/I_o (%)	fwhm
9.360	100	0.358	9.668	100	0.196	9.710	100	0.215
8.052	11	0.680	7.810	5	0.500	7.769	4	0.279
7.675	14	0.478	6.054	24	0.339	6.087	14	0.518
6.794	14	0.519	5.698	14	0.398	5.669	11	0.519
6.375	33	0.399	4.951	13	0.419	4.973	14	0.520
6.054	14	0.298	4.818	46	0.238	4.844	34	0.358
5.698	9	0.265	4.697	10	0.539	4.667	5	0.380
5.343	16	0.439	4.219	6	0.498			
5.199	16	0.457	4.048	9	0.438			
4.823	18	0.459	3.901	9	0.357	3.948	5	0.577
4.711	41	0.216	3.714	8	0.619	3.708	5	0.380
4.480	41	0.299	3.613	8	0.699	3.636	4	0.620
4.122	20	0.678	3.443	4	0.320	3.466	3	5.038
3.847	10	0.080	3.123	10	1.119			
3.717	8	0.140	3.010	10	0.919			
3.493	32	0.799	2.938	9	1.000			
2.795	14	0.938	2.872	6	1.277			

as the terbium compound. Anal. Calcd For $C_{24}H_{20}O_{16}Eu_2 = Eu_2(BDC)_3 \cdot (H_2O)_4$ C, 33.20; H, 2.32; N, 0.00. Found C, 33.55; H, 2.09; N, 0.07. FT-IR (KBr, 3500−400 cm^{-1}) 3460 (br), 3059 (sh), 1690 (sh), 1618 (sh), 1598 (m), 1552 (vs), 1512 (vs), 1433 (s), 1407 (vs), 1315 (sh), 1157 (w), 1144 (w), 1111 (w), 1098 (w), 1032 (w), 894 (w), 834 (w), 762 (m), 584 (m), 565 (m), 538 (m), 512 (m), 440 (w).

Phase purity of the bulk products was confirmed by comparison of the observed and calculated XRPD patterns. The single-crystal structure was determined for $Tb_2(BDC)_3 \cdot (H_2O)_4$ (vide infra), but comparison of the powder patterns indicates that both the terbium and europium compounds are isostructural: Calculated and observed XRPD patterns including *d*-spacing, I/I_o, *hkl*, line widths, and full-width at half-maximum values of the most prominent peaks for both $Tb_2(BDC)_3 \cdot (H_2O)_4$ and $Eu_2(BDC)_3 \cdot (H_2O)_4$ are shown in Table 1.

Thermogravimetric analysis performed under a flow of He on a 28.16 mg crystalline sample of $Tb_2BDC_3 \cdot (H_2O)_4$ showed a weight loss commencing at 63 °C and ending after 3.9 h at 145 °C with a maximum weight loss at 122 °C to give a total weight loss of 2.25 mg (8.0%), which is equivalent to the loss of 4.0 water molecules per formula unit (calcd 8.2%).

$Tb_2(BDC)_3$. A ground microcrystalline sample of freshly isolated and pure $Tb_2(BDC)_3 \cdot (H_2O)_4$ was heated to 115 °C at 0.050 Torr for 2 h to yield the desired dehydrated product. Anal. Calcd for $C_{24}H_{12}O_{12}$-$Tb_2 = Tb_2(BDC)_3$ C, 35.56; H, 1.49; N, 0.00%. Found C, 35.45; H, 1.79; N, 0.10%. The XRPD of this material is shown in Table 2. When this material is exposed to water vapor for 5−15 min, the original powder pattern of the unevacuated material is obtained with some line broadening. The data for this regenerated material are also shown in Table 2. Elemental microanalysis for the regenerated product $C_{24}H_{20}O_{16}$-$Tb_2 = Tb_2(BDC)_3 \cdot (H_2O)_4$: Calcd C, 32.67; H, 2.28; N, 0.00%. Found C, 32.70; H, 2.24; N, 0.25%.

$Tb_2(BDC)_3 \cdot (NH_3)_4$. A freshly isolated sample of $Tb_2(BDC)_3 \cdot (H_2O)_4$ was ground and dehydrated according to the procedure just described. The sample was then placed into a small stainless steel pressure vessel and exposed to 40 psi of anhydrous ammonia gas for 20 min and then stored under ammonia gas atmosphere. XRPD of this material is shown in Table 2. Anal. Calcd for $C_{24}H_{24}O_{12}N_4Tb_2 = Tb_2(BDC)_3 \cdot (NH_3)_4$ C, 32.82; H, 2.75; N, 6.38%. Found C, 31.78; H, 2.92; N, 6.29%.

Sorption Isotherms. Sorption isotherm studies on the evacuated solid were performed by measuring the increase in weight at equilibrium as a function of relative pressure. Sorption measurements were performed using a CAHN 1000 electrobalance using a 1-mg scale (sensitivity 1 μg). A sample with a known weight (typically 120−150 mg) of the as-synthesized starting material was placed in a cylindrical quartz bucket (height = 30 mm, and o.d. × i.d. = 19 × 17 mm) and then heated to 115 °C for 16 h at pressures below 1×10^{-5} Torr to remove the water and produce the dehydrated form. Pressures were measured with two MKS Baratron transducers 622A with the range covering 0−10 and 0−1000 Torr (accuracy 0.25%). The adsorbate was added incrementally and manually, and a point isotherm was recorded

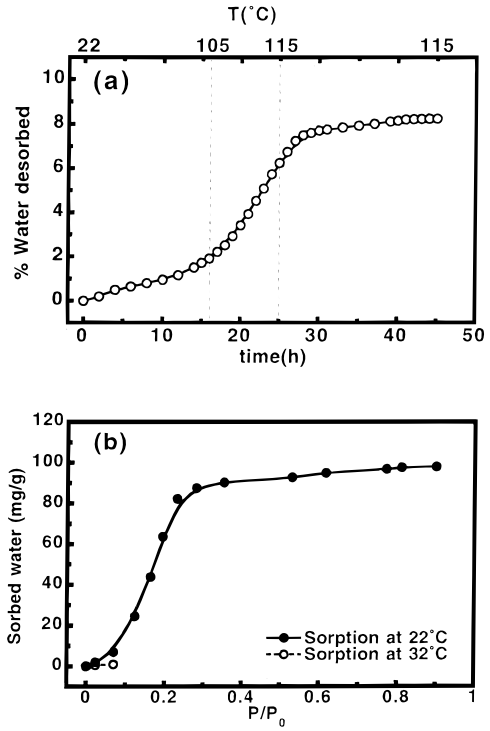

Figure 2. (a) The weight loss measured as a function of time and temperature for as-synthesized $Tb_2(BDC)_3 \cdot (H_2O)_4$. (b) Water sorption isotherm for $Tb_2(BDC)_3$.

when equilibrium was established (when the observed pressure changes were less than 1 mm-Torr/min). Water was of Ultrahigh Quality (UHQ, resistivity 18 MΩ cm at 25 °C), which was obtained using an Barstead Nanopure II system. The N_2 and CO_2 adsorbates were of UHP grade from gas liquid. The temperature of the sample was controlled by a refrigerated bath of liquid nitrogen (−195 °C) and dry ice/acetone (−78 °C) for $N_{2(g)}$ and $CO_{2(g)}$ sorption, respectively. The sorption of ammonia using this technique was not attempted due to its corrosive affects on the apparatus.

Figure 2 shows the weight loss of water from $Tb_2(BDC)_3 \cdot (H_2O)_4$ to yield the dehydrated material, $Tb_2(BDC)_3$, and the water sorption isotherm data. No sorption was observed for $N_{2(g)}$ and $CO_{2(g)}$.

Luminescence Studies. The solid-state excitation−emission spectra of the as-synthesized material were acquired on a Shimadzu RF551 spectrofluorometer with an excitation and emission wavelengths of 545 and 254 nm, respectively. The luminescence lifetime measurements were performed on a Hitachi F4500 spectrofluorometer using slit widths of 5.0 nm for excitation and 2.5 nm for emission. In a typical experiment, the solid sample was layered on a quartz plate and placed into a 1-cm quartz cuvette at 45° and the luminescence collected at 90° from the excitation beam. The sample was excited at 254 nm and the luminescence monitored as a function of time at 543 nm.

The excitation-emmision spectrum for the as-synthesized solid is shown in Figure 3. Samples of the as-synthesized, evacuated, and the ammonia sorbed solids were analyzed for luminescence lifetime. The luminescence decays observed were all single exponential. The decay for each solid was analyzed using a nonlinear least-squares technique on plots of fluorescence intensity (normalized) vs time, allowing the calculation of the decay constants (k) for $Tb_2(BDC)_3 \cdot (H_2O)_4$, $Tb_2(BDC)_3$, and $Tb_2(BDC)_3 \cdot (NH_3)_4$, and their lifetime, $\tau = 1/k$, which are found to be 0.89, 1.35, and 1.00 ms, respectively.

X-ray Data Collection and Reduction. An X-ray single-crystal analysis study was performed on $Tb_2(BDC)_3 \cdot (H_2O)_4$. The experimental details for the structure determination are given in Tables 2, 3, and 4. A fragment of a thin, colorless, bladelike crystal (0.03 × 0.03 × 0.06 mm) was mounted on a glass fiber using Paratone N hydrocarbon oil. All measurements were made on a SMART CCD area detector with graphite-monochromated Mo Kα radiation. The data were collected at a temperature of −109 ± 1 °C. Frames corresponding to an arbitrary

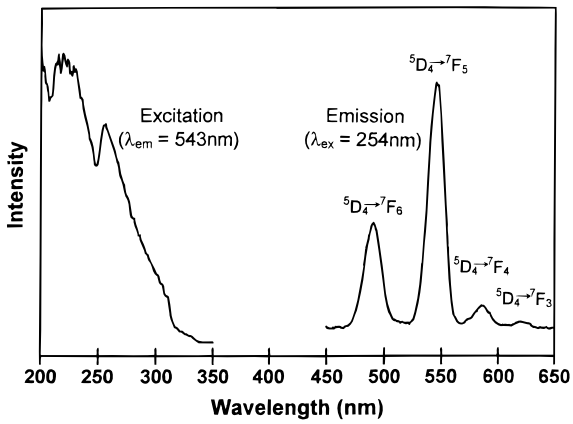

Figure 3. Solid-state excitation−emission spectrum for $Tb_2(BDC)_3 \cdot (H_2O)_4$.

hemisphere of data were collected using ω scans of 0.30° counted for a total 20.0 s per frame. Cell constants and an orientation matrix, obtained from a least-squares refinement using the measured positions of 2287 reflections in the range $3.00 < 2\theta < 45.00°$ corresponded to a primitive triclinic cell.

Data were integrated by the program SAINT to a maximum 2θ values of 49.4° and corrected for Lorentz and polarization effects using XPREP. The data were corrected for absorption based on the comparison of redundant and equivalent reflections as applied using XPREP ($T_{max} = 0.76$, $T_{min} = 0.65$).

Structure Solution and Refinement. The structure was solved using Direct Methods techniques. Terbium and oxygen atoms were refined with the anisotropic displacement parameters, while carbon atoms were refined with isotropic parameters. Attempts to refine anisotropic displacement parameters for carbon yielded unrealistic results. Hydrogen atoms for the organic ligand were included but not refined. The final cycle of full-matrix least-squares refinement was based on 1502 observed reflections ($I > 3.00\sigma(I)$ and $2\theta < 46.4°$) and 130 variable parameters refined to convergence R_1(unweighted, based on F) = 0.036 and $R_w = 0.042$). The maximum and minimum peaks on the final difference Fourier map corresponded to 1.63 and −0.85 e$^-$/Å^3, respectively.

Results and Discussion

Studies performed on the europium and the terbium compounds revealed that they are identical in structure and properties; thus, we will restrict our presentation and discussion to the terbium compounds.

Synthesis and structure of $Tb_2(BDC)_3 \cdot (H_2O)_4$. The hydrothermal reaction of 1,4-benzenedicarboxylic acid (H_2BDC, terephthalic acid) with Tb(III) in the presence of triethylamine yields crystals of a product, which was formulated as $Tb_2(BDC)_3 \cdot (H_2O)_4$ by elemental microanalysis and a single-crystal X-ray diffraction study. Bulk samples of this material are stable in air and are insoluble in water and common organic solvents. Its FT-IR spectrum showed the expected strong characteristic absorptions for the symmetric and asymmetric vibrations of BDC (1610−1550 and 1420−1335 cm^{-1}), and the water ligands (3460 cm^{-1}). It showed no absorptions of any protonated BDC (1715−1680 cm^{-1}), thus confirming complete deprotonation of H_2BDC by triethylamine.[11]

A single-crystal X-ray diffraction study performed on a sample isolated from the reaction product revealed an extended 3-D structure formulated as $Tb_2(BDC)_3 \cdot (H_2O)_4$, which is consistent with that resulting from the elemental microanalysis data. Crystal data, atomic coordinates, and selected bond lengths

(11) (a) Craver, C. D., Ed.; *Desk Book of Infrared Spectra*; The Coblentz Society, Inc.: Kirkwood, MO, 1982. (b) Socrates, G. *Infrared Characteristic Group Frequencies*; John Wiley & Sons, Stonebridge Press: Bristol, 1980.

Table 3. Crystallographic Data for $Tb_2(BDC)_3\cdot(H_2O)_4$

empirical formula	$Tb_2O_{16}C_{24}H_{20}$
formula weight	882.26
crystal color, habit	colorless, bladelike
crystal dimensions	0.03 × 0.03 × 0.06 mm
crystal system	triclinic
space group	$P\bar{1}$
Z	1
a	6.1420(2) Å
b	10.0694(1) Å
c	10.0956(3) Å
α	102.247(2)°
β	91.118(1)°
γ	101.518(2)°
V	596.63(3) Å^3
d_{calc} (g/cm^3)	2.455
μ, mm^{-1}	5.956
$R(R_w)$	0.036(0.042)

Table 4. Atomic Coordinates for $Tb_2(BDC)_3\cdot(H_2O)_4$

atom	*x*	*y*	*z*	B_{eq}
Tb(1)	−0.50260(8)	−0.48328(4)	−0.24484(5)	0.613(11)
O(1)	−0.1161(11)	−0.3880(6)	−0.2891(7)	1.09(14)
O(2)	0.1690(11)	−0.3949(6)	−0.1514(6)	1.01(14)
O(3)	0.2866(11)	0.3376(6)	−0.1650(7)	1.13(15)
O(4)	0.3808(11)	0.3266(6)	0.0455(6)	1.00(14)
O(5)	−0.5154(11)	−0.3007(6)	−0.3502(6)	0.92(14)
O(6)	−0.6075(11)	−0.3806(6)	−0.5711(7)	1.07(15)
O(7)	−0.2351(11)	−0.5943(6)	−0.1333(7)	1.07(14)
O(8)	−0.8366(12)	−0.5886(6)	−0.4108(7)	1.31(15)
C(1)	0.1095(16)	−0.1738(9)	−0.1735(10)	0.79(16)
C(2)	0.2173(16)	−0.1031(9)	−0.0483(10)	0.93(17)
C(3)	0.2683(15)	0.0403(9)	−0.0172(9)	0.44(15)
C(4)	0.2279(16)	0.1174(9)	−0.1095(10)	0.90(17)
C(5)	0.1225(16)	0.0465(9)	−0.2358(9)	0.82(16)
C(6)	0.0580(16)	−0.0974(9)	−0.2646(10)	1.00(17)
C(7)	0.0501(15)	−0.3269(9)	−0.2077(9)	0.61(16)
C(8)	0.3022(16)	0.2703(9)	−0.0742(9)	0.72(16)
C(9)	−0.5251(16)	−0.1352(9)	−0.4840(10)	0.82(16)
C(10)	−0.4271(17)	−0.0254(10)	−0.3781(10)	1.23(18)
C(11)	−0.5990(17)	−0.1109(9)	−0.6051(10)	1.10(17)
C(12)	−0.5509(16)	−0.2807(9)	−0.4647(10)	0.90(17)

Table 5. Selected Bond Lengths and Angles for $Tb_2(BDC)_3\cdot(H_2O)_4$

Distances (Å)			
Tb(1)−O(1)	2.464(7)	Tb(1)−O(2)	2.487(6)
Tb(1)−O(3)	2.303(6)	Tb(1)−O(4)	2.285(6)
Tb(1)−O(5)	2.324(6)	Tb(1)−O(6)	2.264(6)
Tb(1)−O(7)	2.533(6)	Tb(1)−O(8)	2.526(7)
Angles (°)			
O(1)−Tb(1)−O(2)	138.1(2)	O(1)−Tb(1)−O(3)	141.6(2)
O(1)−Tb(1)−O(4)	78.2(2)	O(1)−Tb(1)−O(5)	73.4(2)
O(1)−Tb(1)−O(6)	69.2(2)	O(1)−Tb(1)−O(7)	69.7(2)
O(1)−Tb(1)−O(8)	129.3(2)	O(2)−Tb(1)−O(3)	74.4(2)
O(2)−Tb(1)−O(4)	72.9(2)	O(2)−Tb(1)−O(5)	76.6(2)
O(2)−Tb(1)−O(6)	142.5(2)	O(2)−Tb(1)−O(7)	129.0(2)
O(2)−Tb(1)−O(8)	70.9(2)	O(3)−Tb(1)−O(4)	100.7(2)
O(3)−Tb(1)−O(5)	144.8(2)	O(3)−Tb(1)−O(6)	96.0(2)
O(3)−Tb(1)−O(7)	72.8(2)	O(3)−Tb(1)−O(8)	72.7(2)
O(4)−Tb(1)−O(5)	89.5(2)	O(4)−Tb(1)−O(6)	144.2(3)
O(4)−Tb(1)−O(7)	76.0(2)	O(4)−Tb(1)−O(8)	143.8(2)
O(5)−Tb(1)−O(6)	94.8(2)	O(5)−Tb(1)−O(7)	142.3(2)
O(5)−Tb(1)−O(8)	79.2(2)	O(6)−Tb(1)−O(7)	79.1(2)
O(6)−Tb(1)−O(8)	71.6(2)	O(7)−Tb(1)−O98)	131.3(2)
Tb(1)−O(1)−C(7)	130.4(6)	Tb(1)−O(2)−C(7)	126.5(6)
Tb(1)−O(3)−C(8)	138.7(6)	Tb(1)−O(4)−C(8)	163.7(6)
Tb(1)−O(5)−C(12)	139.6(6)	Tb(1)−O(6)−C(12)	147.6(6)

and angles are presented in Tables 3−5, respectively. A fragment of the structure including the asymmetric unit is shown in Figure 4, where one terbium atom (Tb1), one and a half BDC anions (C1−C8, O1−O4 and C9−C12, O5−O6), and two water

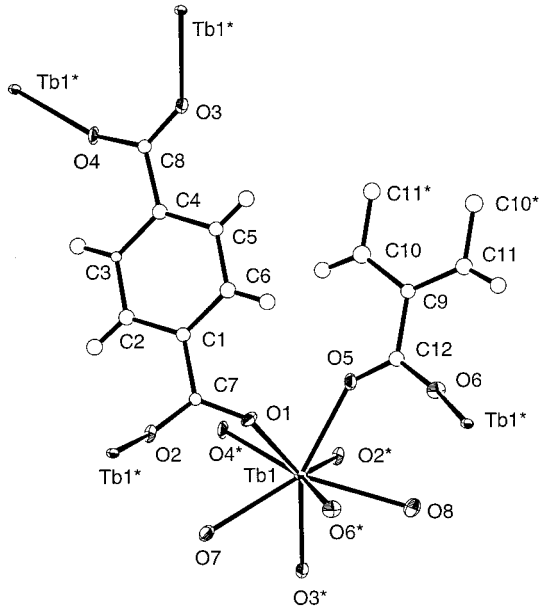

Figure 4. The building block unit including the asymmetric unit present in crystalline $Tb_2(BDC)_3\cdot(H_2O)_4$ with Tb and O atoms represented by thermal ellipsoids drawn at the 50% probability level. Atoms labeled with an additional (*) are symmetry equivalent to those atoms without such designation.

(O7 and O8) molecules are crystallographically unique. The first BDC has no crystallographic symmetry, whereas the second has an inversion center. Each Tb atom is coordinated in a monodentate fashion to six oxygens of BDC anions at a typical Tb−O(carboxylate) distances range (2.464(7)−2.264(6) Å)[10] and two water ligands at slightly longer distance (2.533(6) and 2.526(7) Å) to give an eight-coordinate Tb(III) center. The overall structure can be described in terms of a parallelepipedal motif having a terbium center on each of its eight corners and BDC (C1−C8, O1−O4) on four of its faces, namely, the *ab* and *bc* crystallographic planes and their symmetry equivalent counterparts. In the crystal, the other BDC unit (C9−C12, O5−O6) is responsible for polymerizing the structure into a 3-D condensed network as shown in Figure 5a. It should be noted that the water ligands occupy the *ac* plane, which allows them to point nearly to the center of the parallelepiped, an aspect that is relevant to creating microporosity in that successful removal of the water ligands would result in extended 1-D channels running along the crystallographic *b*-axis as shown in Figure 5b.

Creating Microporosity. Condensed 3-D structures of the type just described are unknown for BDC in the lanthanide metal ion literature, although a few do exist for other carboxylate-containing ligands[10] with only one report[9] showing an example of an open-framework lanthanide−carboxylate network. The structural arrangement just described for the Tb−BDC network is ideally suited for removing water ligands and achieving a microporous framework.

Initial examination of this possibility was performed using thermal gravimetric (TG) measurements on the condensed structure of $Tb_2(BDC)_3\cdot(H_2O)_4$, which showed that 4.0 water molecules per formula unit can be removed at 115 °C from the network to yield the dehydrated solid formulated by elemental microanalysis as $Tb_2(BDC)_3$. The XRPD of this solid has an appearance similar to that of the original solid, which indicates no alteration of the crystal structure topology; however, local distortions within the structure are possible since slight shift and broadening of the diffraction lines have been observed along

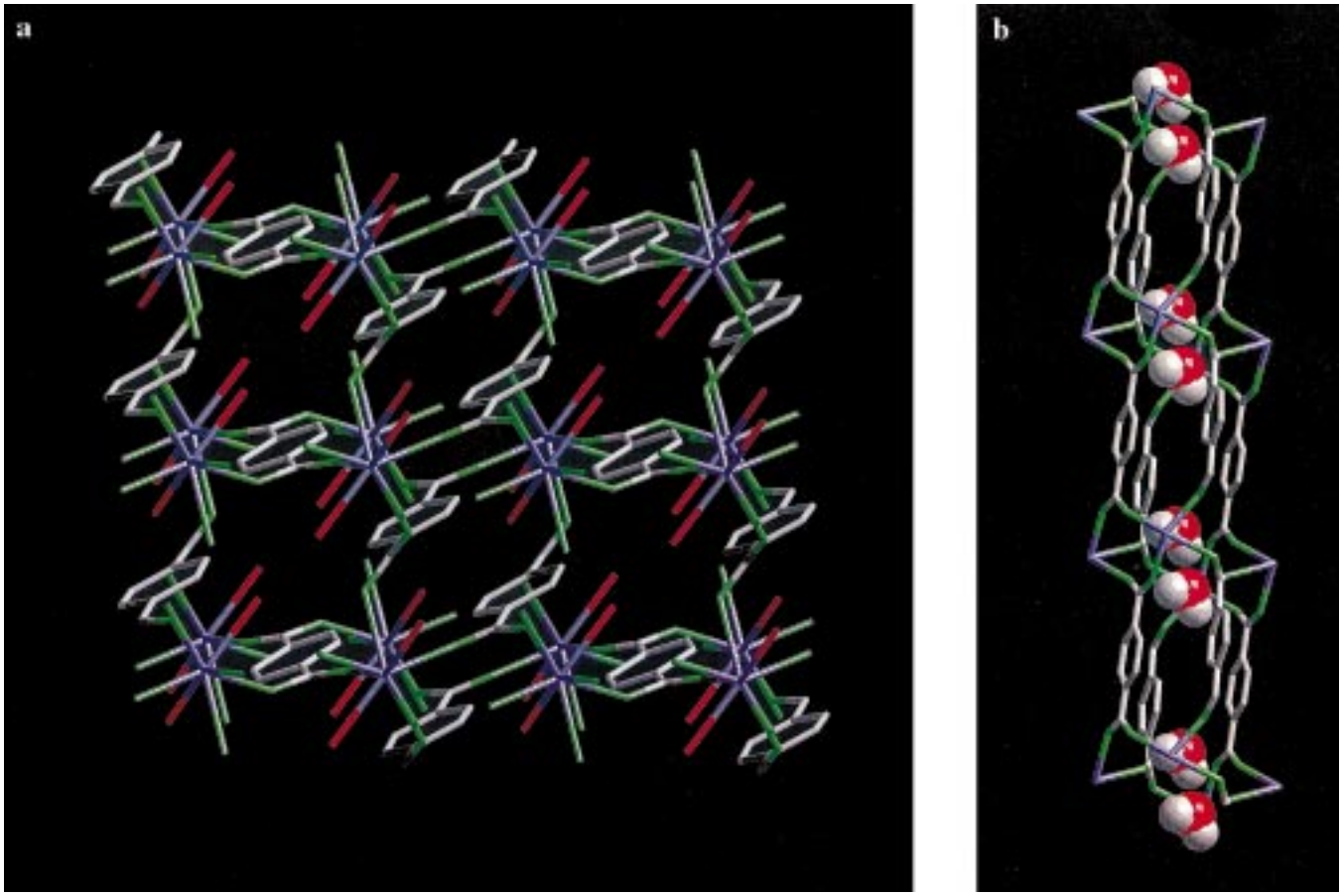

Figure 5. (a) The crystal structure of $Tb_2(BDC)_3 \cdot (H_2O)_4$ shown approximately down the crystallographic *b*-axis, where water ligands are found to point toward the center of 1-D channels. (Tb, blue; C, gray; O (carboxylate), green; and O (water), red). Hydrogen atoms on water and BDC have been omitted for clarity. (b) A view along the crystallographic *a*-axis to emphasize the water distribution into the channels.

with the emergence of new small diffraction lines (Table 2). This phenomenon is commonly observed in zeolites and molecular sieves,[12] and it is attributed to distortions in the pore structure and often results in slight lowering of the overall symmetry of the structure due to the evacuation of the pores: such distortions, although significant, do not preclude microporosity in porous solids. It is worth noting that the microporous solid thus produced, $Tb_2(BDC)_3$, does not lose weight upon heating to 450 °C as shown by the TG data, indicating a stable structural arrangement according Figure 5b. The reintroduction of water to the $Tb_2(BDC)_3$ solid yields the starting material with exactly the same formulation as shown by the sorption data (Figure 2b) and elemental microanalysis (see Experimental Section). This material also shows an XRPD similar to that of the original solid as shown in Table 1, which confirms the reversibility of the dehydration process.

Encouraged by the stability of this network and the reversibility of the hydration−dehydration process, we sought to further confirm the permanent microporosity of $Tb_2(BDC)_3$ by measuring its gas sorption isotherm. Initially, the original solid was evacuated under vacuum at 115 °C to remove the water ligands, and the weight loss was monitored as a function of time as shown in Figure 2a. A maximum loss of 8% was observed, confirming the TG data that four water molecules per formula unit were removed. Water was reintroduced in increments at room temperature and the corresponding weight gain monitored by an electromicrobalance. Figure 2b shows a type V isotherm behavior for $Tb_2(BDC)_3$: an initial weak uptake of water at very low relative pressure followed by a rapid uptake reaching a limit value at relative pressure of 0.3 and then the eventual saturation of the pores. The absence of any other uptake at relative high pressure (>0.60) proves that the micropores are completely filled and that the sorbed water is not exposed at the surface of the particles, as the presence of such water would have been observed in the isotherm behavior as an increased uptake by capillary condensation.[13]

The rapid uptake behavior of $Tb_2(BDC)_3$ is characteristic of strong sorbate−sorbent interaction. This is anticipated since the pores are decorated with coordinatively unsaturated terbium centers and water is expected to chemically bind to Tb upon its introduction into the pores. To gain some insight into the behavior of water sorption within the channels, the uptake of this material was examined at low relative pressure (<0.1) (Figure 2b). Here, the water uptake was monitored as a function of temperature and found to decrease with increasing temperature, which is indicative of an activation mechanism involving the metal sites within the pores rather than the usual activation mechanisms by diffusion in restricted pores. This is consistent with water molecules filling the pores and inducing a coordination change around Tb, thereby creating high-energy binding sites on the pore surface for water ligands.

The monolayer capacity is very difficult to deduce from this type of isotherm; however, the value at the plateau can be used

(12) Breck, D. W. In *Zeolite Molecular Sieves, Structure, Chemistry, and Use*; John Wiley & Sons: New York, 1974.

(13) (a) According to IUPAC classification: Sing, K. S. W.; Everett, D. H.; Haul, R. A. W.; Moscou, L.; Pierotti, R. A.; Rouquerol, J.; Siemieniewski, T. *Pure Appl. Chem.* **1985**, *57*, 603−619. (b) Gregg, S. J.; Sing, K. S. W. *Adsorption, Surface Area, Porosity*, 2nd ed.; Academic Press: London, U. K., 1982.

to estimate the total pore volume, assuming the state of water near saturation as a liquid. A pore volume of 0.099 cm^3/g (0.223 cm^3/cm^3) can be derived from the amount sorbed near saturation pressure (98.78 mg/g of adsorbent). The pore volume of this material is strikingly similar to that observed for hydrated zeolites with narrow pores such as Analcime, where water is coordinated to the cations with no hydrogen bonding observed by water molecules, a structural environment analogous to that of the $Tb_2(BDC)_3$ microporous material.[12] Attempts to measure the isotherm using CO_2 and N_2 gases revealed no uptake due to their exclusion from the pores, since their kinetic diameters (3.30 and 3.64 Å, respectively) are larger than that of water (2.60 Å).[12,13]

Although the corrosive nature of ammonia prohibited the measurement of its sorption isotherm, its introduction into the microporous framework of $Tb_2(BDC)_3$ produced a solid formulated by elemental microanalysis as $Tb_2(BDC)_3\cdot(NH_3)_4$, which essentially has the same structure as the as-synthesized solid (compare Tables 1 and 2). This is not surprising since the kinetic diameter of ammonia (2.60 Å) is complementary to the size of the pores resulting in its sorption and ligation to Tb in exactly the expected ratio ($2NH_3$:1Tb).

Luminescence Lifetime Study. The sensitized emission of lanthanide−aromatic complexes is a common occurrence in rare-earth chemistry. It is essential to use these chromophoric ligands to create highly fluorescent materials, due to the characteristic low absorbance coefficients of europium and terbium ($<1\ M^{-1}\ cm^{-1}$). The π to π^* energy transfer from the ligand to the metal in these types of complexes is thought to go through an intramolecular path which is followed by the characteristic luminescence of the metal.[14] The $Tb_2(BDC)_3$ microporous solid is well-suited for such studies due to its expected long-lived luminescence and the opportunity to examine its optical sensitivity to different guest species.[14e]

Excitation of the as-synthesized solid at 254 nm reveals the expected $^5D_4 \rightarrow {}^7F_n$ transitions with $n = 6, 5, 4, 3$ as shown in Figure 3. Due to the low resolution of the spectrometer, no further splitting of the peaks was visible. Samples of the as-synthesized, evacuated, and the ammonia-sorbed solids were analyzed for luminescence lifetime by monitoring the decay of the $^5D_4 \rightarrow {}^7F_5$ emission line at 543 nm. The decay constants (k_{obs}) for each solid were found to decrease in the sequence: $Tb_2(BDC)_3\cdot(H_2O)_4$ ($1.13 \pm 0.02\ ms^{-1}$) > $Tb_2(BDC)_3\cdot(NH_3)_4$ ($1.00 \pm 0.01\ ms^{-1}$) > $Tb_2(BDC)_3$ ($0.74 \pm 0.01\ ms^{-1}$), consistent with the fact that −OH oscillators are better than −NH oscillators at quenching luminesence.[14e,f] A method employing a plot of Δk_{obs} vs the number of coordinated water (q) has been devised and tested to allow the determination of the number of water ligands coordinated to metal ions in extended and molecular systems.[14e,g] Application of this method to the present case by comparing k_{obs} of the hydrated and dehydrated forms of the Tb−BDC framework gives a Δk_{obs} of 0.39 ms^{-1}, which indicates that two water molecules ($q = 2$) are linked to each metal ion. This is in agreement with the X-ray analysis and sorption data as well as with numerous studies performed on Tb(III) complexes and solids.[14g] Given that distinctly different decay constants are observed based on the presence or absence of guests in this framework, and the apparent periodicity of accessible metal sites within the pores, it is not unreasonable to anticipate the use of such materials in shape-selective and metal-site specific chemical sensing. Current experiments focus on the generation of materials with larger pores that have accessible metal centers of the type reported here.

Summary

This study demonstrates a strategy for transforming condensed structures into microporous networks. The multi-monodentate functionality of 1,4-benzenedicarboxylate is essential in restricting the coordination around the terbium center in the condensed, extended 3-D structure of $Tb_2(BDC)_3\cdot(H_2O)_4$ and thus allowing the ligation of terminal water and ammonia molecules. The successful removal of such ligands, by thermally treating the resulting solid, yields a $Tb_2(BDC)_3$ microporous phase having extended 1-D channels decorated with accessible metal sites that potentially can be considered as fluorescent probes for detecting small molecules. The extension of this work to include the study of these metal sites as Lewis acid sites for low-temperature catalysis is in progress.

Acknowledgment. The financial support of this work by the National Science Foundation (Grant CHE-9522303), Department of Energy (Division of Chemical Sciences, Office of Basic Energy Sciences, Grant DE-FG03-98ER14903) and Nalco Chemical Company and the crystallographic work provided by Dr. Fred Hollander (UC-Berkeley) are gratefully acknowledged.

Supporting Information Available: Crystallographic data for $Tb_2(BDC)_3\cdot(H_2O)_4$, including a crystal structure analysis report, positional parameters, thermal parameters, and interatomic distances and angles (PDF). This material is available free of charge via the Internet at http://pubs.acs.org.

JA983577D

(14) (a) Bünzli, J.-C. G.; Choppin, G. R., Eds.; *Lanthanide Probes in Life, Chemical and Earth* Sciences; Elsevier: Amsterdam-Oxford-New York-Tokyo, 1989. (b) Barthelemy, P. P.; Choppin, G. R. *Inorg. Chem.* **1989**, *28*, 3354−3357. (c) Horrocks, W. DeW., Jr.; Arkle, V. K.; Liotta, F. J.; Sudnick, D. R. *J. Am. Chem. Soc.* **1983**, *105*, 3455−3459. (d) Horrocks, W. DeW., Jr.; Sudnick, D. R. *Science* **1979**, *206*, 1194−1196. (e) Horrocks, W. DeW., Jr.; Albin, M. *Prog. Inorg. Chem.* **1984**, *31*, 1−103. (f) Eaton, D. F. *Pure Appl. Chem.* **1990**, *62*, 1631−1648. (g) Horrocks, W. DeW., Jr.; Sudnick, D. R. *J. Am. Chem. Soc.* **1979**, *101*, 334−340.